**RESEARCH ARTICLE**

**Key Points:**
- Statistical model relating micro-CT structure to SMP force for many snow data
- New method to retrieve density, correlation length, and SSA in the field
- Efficient retrieval of spatial variability and 2-D stratigraphy of snow

**Correspondence to:**
M. Schneebeli,
schneebeli@slf.ch

# Density, specific surface area, and correlation length of snow measured by high-resolution penetrometry

**Martin Proksch[1,2], Henning Löwe[1], and Martin Schneebeli[1]**

[1]WSL Institute for Snow and Avalanche Research SLF, Davos, Switzerland, [2]Institute of Meteorology and Geophysics, University of Innsbruck, Innsbruck, Austria

**Abstract** Precise measurements of snow structural parameters are crucial to understand the formation of snowpacks by deposition and metamorphism and to characterize the stratigraphy for many applications and remote sensing in particular. The area-wide acquisition of structural parameters at high spatial resolution from state-of-the-art methods is, however, still cumbersome, since the time required for a single profile is a serious practical limitation. As a remedy we have developed a statistical model to extract three major snow structural parameters: density, correlation length, and specific surface area (SSA) solely from the SnowMicroPen (SMP), a high-resolution penetrometer, which allows a meter profile to be measured with millimeter resolution in less than 1 min. The model was calibrated by combining SMP data with 3-D microstructural data from microcomputed tomography which was used to reconstruct full-depth snow profiles from different snow climates (Alpine, Arctic, and Antarctic). Density, correlation length, and SSA were derived from the SMP with a mean relative error of 10.6%, 16.4%, and 23.1%, respectively. For validation, we compared the density and SSA derived from the SMP to traditional measurements and near-infrared profiles. We demonstrate the potential of our method by the retrieval of a two-dimensional stratigraphy at Kohnen Station, Antarctica, from a 46 m long SMP transect. The result clearly reveals past depositional and metamorphic events, and our findings show that the SMP can be used as an objective, high-resolution tool to retrieve essential snow structural parameters efficiently in the field.

## 1. Introduction

Though substantial advances have been made to develop an international system for snow classification [*Fierz et al.*, 2009], the relation of stratigraphic and morphometric parameters to physical properties of snow is far from being solved. However, it is commonly agreed that objective measurements of snow stratigraphy in terms of density and grain size constitute an essential step to characterize the majority of physical properties. With density and specific surface area (SSA), as the most prominent objective morphometric measures, key properties as thermal conductivity, dielectric permittivity, or air permeability can be computed [*Arons and Colbeck*, 1995; *Mätzler*, 1996; *Calonne et al.*, 2012]. Although these two morphometric properties are strictly not sufficient to characterize snow microstructure [*Löwe et al.*, 2013], they provide a valuable first approximation for quantitative means. For microwave models [*Mätzler*, 1999; *Pulliainen et al.*, 1999; *Picard et al.*, 2013], density and grain size constitute the essential input parameters. Noteworthy, some microwave models such as Microwave Emission Model of Layered Snowpacks (MEMLS) [*Wiesmann and Mätzler*, 1999] use the correlation length instead of the SSA as a prominent, alternative characterization of grain size and density.

Traditionally, the stratigraphy of a snowpack is characterized by careful estimates of grain size, snow type, and density in classified layers along a quasi one-dimensional vertical line. These manual measurements are time consuming, and naturally limited in spatial resolution. Density resolution is limited by the cutting device and always larger than about 3 cm. Moreover, traditional grain size measurements are subjective and depend on the observer [*Painter et al.*, 2007]. To overcome this limitation, various field methods were developed in the last decade to retrieve an objective grain size from in situ measurements of the snowpack in the field. Techniques, such as near-infrared photography (NIP) [*Matzl and Schneebeli*, 2006], shortwave-infrared (SWIR) photography [*Montpetit et al.*, 2012], infrared profilers [*Arnaud and Picard*, 2011], contact spectroscopy [*Painter et al.*, 2007], and SWIR reflectance [*Gallet et al.*, 2009], are able to provide the optically equivalent diameter objectively. The spatial resolution of these methods varies between a few millimeters and centimeters. These methods are clearly superior to traditional snow characterization

methods which are not able to capture the microstructure with sufficient detail. For all of these methods, measurement time is, however, a critical resource, given the necessity of sampling the footprints of, e.g., airborne or spaceborne remote sensing products at sufficient detail. In the end, always a trade-off must be made between measurement accuracy and available time.

Measurement time becomes even more important in view that many applications actually require a two-dimensional characterization of the stratigraphy to track spatial, subsurface features. This is particularly important for weak layers in avalanche forecasting [*Schweizer et al.*, 2003], ice lenses for microwave remote sensing [*Durand et al.*, 2008], or snow accumulation [*Scambos et al.*, 2012]. Then, it is inevitable to have high-resolution methods which are able to effectively "scan" large parts of the subsurface. Along these lines, near-infrared (NIR) photography was used qualitatively to provide a clear image of spatial variability at the scale of several meters [*Tape et al.*, 2010; *Matzl and Schneebeli*, 2006]. Also, *Rutter et al.* [2014] demonstrate the importance of a two-dimensional stratigraphy of snow unambiguously. Though optical grain size was determined objectively, the method still lacks a convenient retrieval of density, which must be measured by volumetric sampling and weighing. There is yet no method known to objectively quantify the spatial variability of density. Dielectric methods are not much faster than volumetric sampling [*Denoth et al.*, 1984]. Radar does provide stratigraphic information [*Arcone et al.*, 2012; *Marshall et al.*, 2007]; however, a full reconstruction of the density profile is still missing [*Schmid et al.*, 2014]. In addition, grain size cannot be measured by radar. Overall, a method which gives a fast, combined measurement of density and SSA (or correlation length) is not yet available.

It is the objective of the present paper to develop a method that overcomes some of the limitations described above and enables an efficient and objective retrieval of the two-dimensional stratigraphy of a snowpack in terms of the key parameters density, specific surface area, and correlation length. We have combined the efficiency of SnowMicroPen (SMP) penetration measurements with state-of-the-art microstructure characterization by microcomputed tomography (micro-CT). The SMP [*Schneebeli et al.*, 1999] was specifically designed to obtain high-resolution profiles at fast acquisition times. Full-meter penetration profiles of the snowpack can be taken within a minute, and this has been exploited in various applications [*Sturm and Benson*, 2004; *Kronholm et al.*, 2004; *Bellaire et al.*, 2009; *Reuter and Schweizer*, 2012]. However, the interpretation of the penetration force in terms of microstructural parameters is challenging [*Johnson and Schneebeli*, 1999; *Schneebeli*, 2001] and less obvious as the relation of the SSA to optical methods mentioned above. We have used an existing stochastic approach to the penetration signal [*Löwe and van Herwijnen*, 2012] which provides a minimal physical picture of the penetration process in terms of a microstructural length scale, the element size $L$. Though the model gives an unambiguous recipe for how $L$ can be retrieved from the penetration signal, its relation to an objective geometrical length scale of the 3-D microstructure is still missing. Therefore, we made use of micro-CT as a calibration tool and established the connection between the SMP parameters and micro-CT measured quantities as density, SSA, and correlation length on a statistical basis. To this end we measured the microstructure of several full-meter profiles of snow from three different snow climatological sites (Alpine, Arctic, and Antarctic) by micro-CT. The comparison to parallel SMP measurements provides the basis for our regression model.

Our method gives access to a two-dimensional quantitative stratigraphy without digging a snow pit, providing new insight into the processes in any snowpack [*Benson*, 1971]. We demonstrated this by the reconstruction of a two-dimensional stratigraphy from Antarctica, which allows a quantitative and deeper understanding of depositional and metamorphic processes.

The paper is organized as follows: In section 2 we recap the definition of the relevant micro-CT and SMP parameters and describe their retrieval from individual snow samples. In section 3 we present the different data sets used here (Alpine, Arctic, and Antarctic snow) and highlight particularities of the retrieval of micro-CT and SMP parameters for full-depth profiles in different data sets. In section 4 we present the development of the statistical model, its validation, and the retrieval of the two-dimensional stratigraphy at Kohnen station as an application of the method. The findings are discussed in section 5.

## 2. Methods

In the following we summarize the key quantities which are derived from the 3-D microstructure of micro-CT images (section 2.1) and from the force-displacement data of the SMP (section 2.2). The statistical model is based on a regression analysis between these quantities.

## 2.1. Microcomputed Tomography

### 2.1.1. Density and Two-Point Correlation Function

Micro-CT characterizes the microstructure of snow as a two-phase material. The microstructure is reconstructed within a representative cubic volume $V$ of side length $w^{(ct)}$ which is typically in the order of a few millimeters to centimeters. The reconstructed binary image contains the full microstructure in terms of the so-called indicator function [e.g., *Torquato*, 2002] $\phi_i(\mathbf{r})$ which is $\phi_i(\mathbf{x}) = 1$ for points $\mathbf{x} \in V$ in the ice phase and $\phi_i(\mathbf{x}) = 0$ for points in the air phase. The volume fraction of ice can be computed by a volume average

$$\phi_i = \overline{\phi_i(\mathbf{x})} \tag{1}$$

which is denoted by an overbar. The mass density $\rho$ of snow is then trivially related to the volume fraction by $\rho = \rho_{ice}\,\phi_i$ in terms of the density $\rho_{ice} = 917 \text{ kg m}^{-3}$ of ice.

Additional structural information can be derived from the two-point correlation function $C(\mathbf{r})$ with lag distance $\mathbf{r}$

$$C(\mathbf{r}) = \overline{(\phi_i(\mathbf{x} + \mathbf{r}) - \phi_i)\left(\phi_i(\mathbf{x}) - \phi_i\right)} \tag{2}$$

which is the autocovariance of the ice phase indicator function. Below we use the correlation function $C(\mathbf{r})$ to compute both the SSA and the correlation length from the micro-CT image.

### 2.1.2. Specific Surface Area

For isotropic, porous materials the correlation function $C(r) = C(|\mathbf{r}|)$ depends solely on the magnitude $r = |\mathbf{r}|$ of the lag. The SSA is then related to the derivative of $C(r)$ at the origin, $l_c$, via [*Debye et al.*, 1957]

$$l_c = \left( \left. \frac{dC(r)}{dr} \right|_{r=0} \right)^{-1} \tag{3}$$

and

$$SSA = \frac{4(1 - \phi_i)}{l_c} \tag{4}$$

in terms of the volume fraction $\phi_i$. This relation can be generalized for anisotropic media such as snow [*Riche and Schneebeli*, 2013], if the derivative with respect to $r$ is subsequently averaged over all orientations [*Berryman*, 1987]. Practically, we have computed the derivatives of $C(\mathbf{r})$ in each Cartesian coordinate direction [*Löwe et al.*, 2011] and averaged them arithmetically. We use the SSA in terms of surface area per ice volume.

### 2.1.3. Exponential Correlation Length

The SSA characterizes the behavior of the correlation function only at the origin and thus contains structural information only from the smallest scales. For various physical properties such as electromagnetic wave interaction, it is advantageous to define a length scale which characterizes the correlation function as a whole [*Debye et al.*, 1957; *Mätzler*, 2002], and not only at the origin. The simplest approach is to fit the entire correlation function to an exponential form

$$C(\mathbf{r}) = C_0 \exp(-|\mathbf{r}|/l_{ex}) \tag{5}$$

where $l_{ex}$ is the exponential correlation length. Again, we take into account that snow is anisotropic and fit the anisotropic correlation function $C(\mathbf{r})$ in each Cartesian coordinate direction to an exponential [cf. *Löwe et al.*, 2013]. A single value for the exponential correlation length is obtained by arithmetically averaging over all directions.

### 2.1.4. Processing Details

For the characterization of snow by micro-CT we have used a SCANCO Medical micro-CT 40 and a micro-CT 80, operated in the cold lab at −20°C. Generally, micro-CT scans were performed with different nominal resolutions (voxel size) ranging from 10 μm for new snow to 25 μm for depth hoar. The size of the evaluated volumes to calculate the correlation functions ranges from $w^{(ct)} = 2.56$ mm to $w^{(ct)} = 10$ mm. The gray scale image resulting from each scan was filtered using a Gaussian filter ($\sigma = 1$ voxel, support = 2 voxel) and then segmented into a binary image. Thresholds were chosen by matching the volumetric density of the binary image with the gravimetric density of the samples weighted with a precision scale. For those samples which
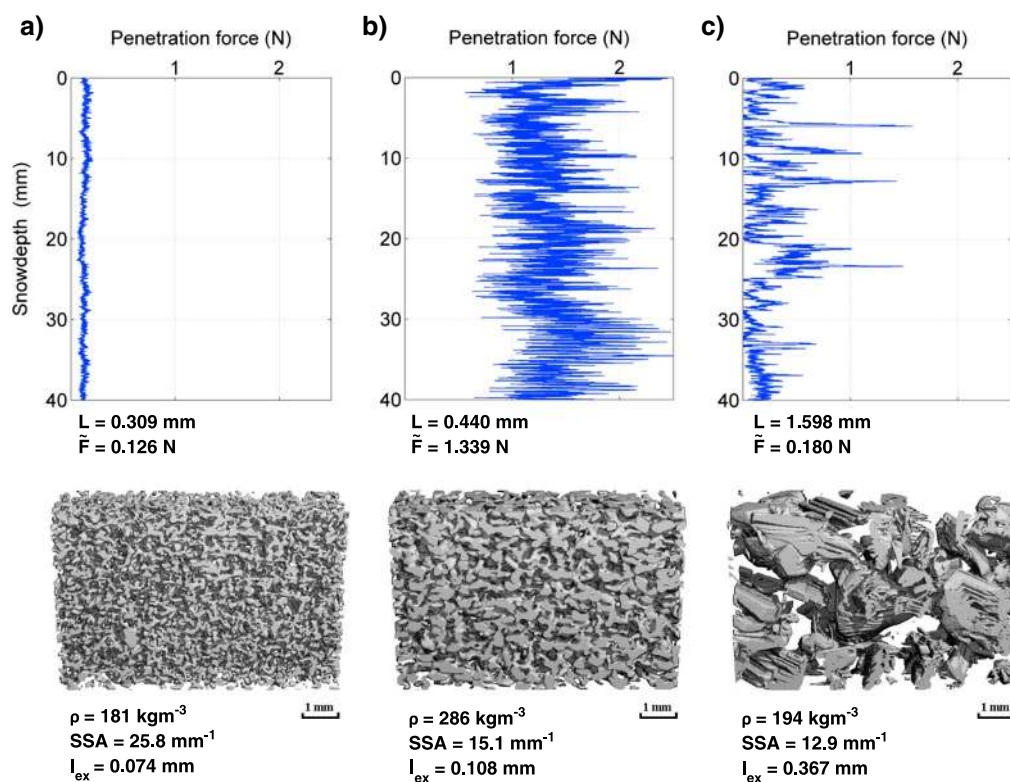
**Figure 1.** (top row) SMP force signal and (bottom row) micro-CT 3-D reconstruction of the snow structure for three typical snow types, with corresponding $L$, $\tilde{F}$, $l_{ex}^{(ct)}$, SSA$^{(ct)}$, and $\rho^{(ct)}$ values: (a) low-density new snow with flat SMP force signal, (b) dense melt refrozen structure with higher mean penetration force and noisy signal, and (c) medium-density depth hoar crystals with distinct peaks in the SMP force, which reaches zero if the SMP tip enters the pore space between the large-depth hoar crystals.

were cast in Diethly-Phthalate (DEP), we followed *Heggli et al.* [2009]. In this case the threshold for image segmentation was chosen as the minimum between the DEP peak and the air peak in the histogram of the gray scale image. The error in density of cast samples compared to uncast samples found by *Heggli et al.* [2009] is 3.15% on average. After segmentation the correlation functions were computed from the binary image and the parameters $\rho^{(ct)}$, SSA$^{(ct)}$, and $l_{ex}^{(ct)}$ were derived as described. Three examples of the micro-CT data are given in Figure 1 (bottom row), which shows the binary images with the corresponding $\rho^{(ct)}$, SSA$^{(ct)}$, and $l_{ex}^{(ct)}$ values.

## 2.2. Snow Micropenetration
### 2.2.1. Structural Element Size
In contrast to micro-CT imaging, which yields almost unambiguous information about the microstructure, it is far less straightforward to interpret the fluctuating force signal obtained from SMP measurements in terms of snow microstructure. A stochastic model was developed by *Löwe and van Herwijnen* [2012], which interprets the penetration force as a Boolean model of noninteracting elastic-brittle, mechanical, elements. The elements are distributed randomly in three-dimensional space according to a Poisson point process.

The independent superposition of deflection and rupture of individual elements at random positions upon penetration leads to a one-dimensional shot-noise process as a model for the fluctuating force signal. The model constitutes a convenient reinterpretation of *Marshall and Johnson* [2009] and enables an analytical procedure to estimate the mechanical parameters and the intensity $\lambda_{3\text{-}D}$ of the underlying Poisson process from the penetration force correlation function. The intensity $\lambda_{3\text{-}D}$ represents an average number density of elements in three-dimensional space and the associated length scale $L = \lambda_{3\text{-}D}^{-1/3}$ can thus be interpreted as a typical distance between the structural elements. The scale $L$ is referred to as structural element length and constitutes the key length scale of the penetration process. Note that $L$ is derived from purely mechanical data without any a priori connection to structural length scales derived from micro-CT.

As outlined by *Löwe and van Herwijnen* [2012], the relevant parameters are computed from the two-point force correlation function $A$ of the penetration force $F(z)$ with lag distance $z$ from

$$A(z) = \overline{(F(z' + z) - \overline{F})(F(z') - \overline{F})} \tag{6}$$

in a window of size $w^{(smp)}$. Here $\overline{F}$ represents the mean of the SMP force in that window. The intensity $\lambda_{3\text{-}D}$ of the Poisson process

$$\lambda_{3\text{-}D} = \frac{4 \overline{F}^2}{3 \sigma(F) \delta S} \tag{7}$$

is computed from the mean and the variance $\sigma(F)$ of SMP force in each window, where $S$ is the (projected) cone area of the SMP tip. The parameter $\delta$ denotes the deflection at rupture which can be estimated from the slope of the force correlation function $A(z)$ at the origin

$$\delta = -\frac{3A(0)}{2A'(0)} \tag{8}$$

For further details of the parameter estimation we refer to *Löwe and van Herwijnen* [2012].

### 2.2.2. Signal Processing

The SMP measures the force in a range from 0.01 N for soft snow up to 75 N for very hard snow down to a maximum depth of 1.7 m, with a constant measurement speed of 20 mm s$^{-1}$. Generally, only SMP signals were retained which were classified "C1" according to the SMP signal quality classification of *Pielmeier and Marshall* [2009], i.e., signals containing trends or offsets in the absolute SMP force or disturbances in the SMP force microvariance were excluded from the analysis. Furthermore, all nonstationary signals, i.e., signals which showed distinct crusts or ice lenses, indicated by rapid changes in penetration force by a factor hundred within less than 1 mm were excluded, as for the stochastic parameter retrieval the penetration force is assumed to be stationary [*Löwe and van Herwijnen*, 2012]. For this study, the SMP parameter profiles were always filtered with a sliding window size of $w^{(smp)} = 2.5$ mm width and 50% overlap, yielding an estimate of the SMP parameters $L$ and $\tilde{F}$ for each window. Three typical examples of SMP data are given in Figure 1 (top row), which shows the derived $L$ and $\tilde{F}$ values.

### 2.2.3. Relating Micro-CT and SMP Quantities

To motivate the underlying idea of the statistical models used later, we provide a simple picture how the penetration process in snow might be related to the structural length scales derived from tomography. Figure 2 (left) shows the force signal of the penetration process in snow from *Schneebeli and Johnson* [1998], with $L$ being the mean distance between two rupturing elements. On the right side, a plane section of real snow and the path of a hypothetical, point-like penetrometer into that snow structure is shown. Making contact with the structure at point 1 corresponds to the first elastic increase of the force in the left schematic. Then, after a small elastic deflection of length $\delta$, the blue unit breaks, corresponding to the force drop on the left. One assumption of the model [*Löwe and van Herwijnen*, 2012] is that broken parts do not further influence the force signal. Consistent with that would be a next contact of the tip with the structure at point 2. Therefore, we could assign the length $L$ as shown in the right part of the figure. In an isotropic structure this length (averaged over consecutive events) would exactly give $L \sim 1/\text{SSA}$, according to the principles of stereology. Since SSA and correlation length are not completely independent, a similar reasoning could be anticipated for the correlation length.

The true penetration process is indeed more complicated but we will be guided by the above idea of relating structural length scales to penetrometer length scales later in the statistical model. As an additional phenomenological input parameter for the statistical model we shall use the median of the penetration force $\tilde{F}$ which was shown to be correlated to snow density by *Pielmeier* [2003].

## 3. Data

The basic requirement for each data set was the availability of simultaneous SMP and micro-CT measurements. To cover a large range of snow types we compiled three different data sets consisting of Alpine, Arctic, and Antarctic snow. Snow densities range from 73 to 574 kg m$^{-3}$, values of SSA from 5.8 to 50.8 mm$^{-1}$, and values of correlation length from 0.054 and 0.442 mm, respectively. The differences in the data sets with respect to sampling design, resolution, and sample sizes are described below. An overview of the data can be found in Table 1, an overview of the sampling designs in Figure 3.
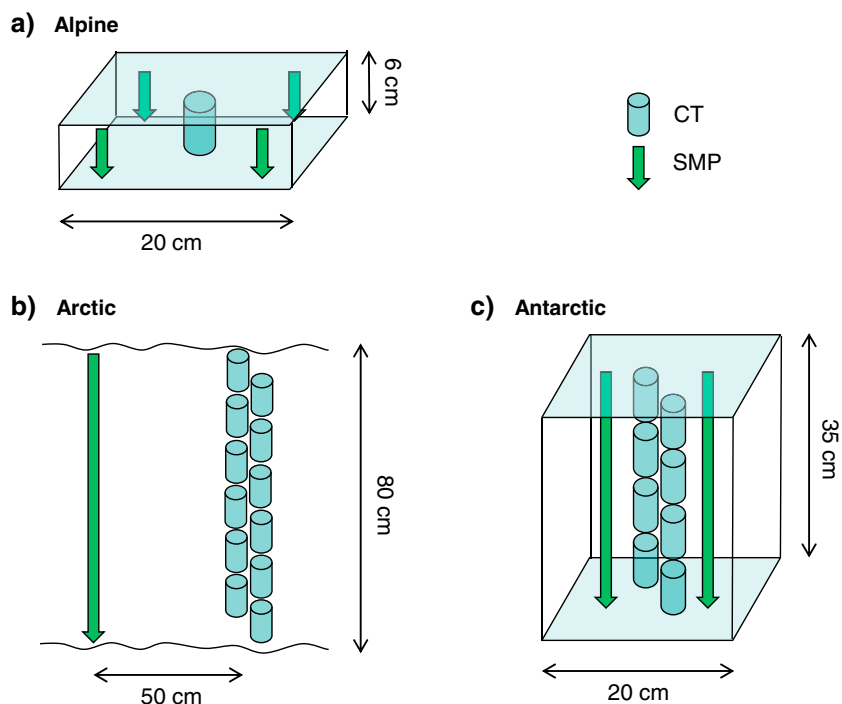
**Figure 2.** Sketch of the sampling designs, showing the dimensions of the snow samples and the locations of the SMP and micro-CT measurements. (a) Design for Alpine snow samples, (b) for the Arctic snow samples, and (c) for the Antarctic snow samples.

### 3.1. Alpine Snow

The Alpine snow data set was gathered by *Riche and Schneebeli* [2013]. It consists of natural snow samples taken under various snow conditions in the winters 2009/2010 and 2010/2011, as well as sieved nature-identical snow from a snowmaker [*Schleef et al.*, 2014]. The Alpine data set represents the most diverse one in terms of snow types.

The snow samples were cut to a size of 20 cm × 20 cm × 6 cm. The size was chosen to be large enough to extract a micro-CT sample in the center and conduct up to four SMP measurements around the micro-CT sample, Figure 2a. SMP and CT measurements were performed simultaneously in the cold lab in Davos. The micro-CT values of the structural parameters for each Alpine snow sample were obtained from a single micro-CT scan with cube size $w^{(ct)} = 1$ cm.

The values of $L$ and $\tilde{F}$ of each SMP measurement (obtained with a window size of $w^{(smp)} = 2.5$ mm with 50% overlap) were averaged over the sample height to overcome spatial variability in the vertical direction. Then the vertically averaged $L$ and $\tilde{F}$ values of the up to four neighboring SMP measurements of each snow sample were averaged again to overcome spatial variability in the horizontal direction. The natural snow samples of the Alpine data set showed a slight stratification and small changes in the SMP penetration force in both vertical and horizontal direction.

### 3.2. Antarctic Snow

The Antarctic data set consists of snow sampled on two expeditions, the first one to Point Barnola (75.70°S, 123.25°E), East Antarctica, during the austral summer 2011–2012, and the second one to Kohnen Station (75.00°S, 00.07°E), Dronning Maud Land, East Antarctica, during the austral summer 2012–2013.

**Table 1.** Summary of the Data Sets Used in This Study

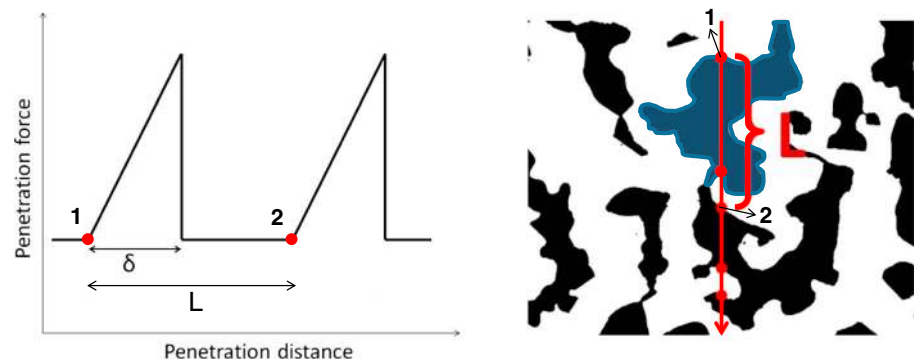| Data Set | Origin | Type | Distance SMP to Micro-CT | SMPs per Micro-CT | $\rho$ (kg m$^{-3}$) | SSA (mm$^{-1}$) | $l_{ex}^{(ct)}$ (mm) |
|---|---|---|---|---|---|---|---|
| Alpine | Davos, CH | Sampled in cold lab | < 10 cm | ≤ 4 | 107–377 | 7.5–50.8 | 0.054–0.356 |
| Arctic | Sodankylä, FI | Casted in field | < 50 cm | 1 | 73–343 | 6.9–47.9 | 0.055–0.390 |
| Antarctic | Kohnen Station and Point Barnola, AQ | Sampled in cold lab | < 20 cm | 2 | 228–573 | 5.8–16.7 | 0.078–0.442 |

**Figure 3.** (left) Schematic model of the penetration process in snow from *Schneebeli and Johnson* [1998], with *L* being the mean distance between two rupturing elements. (right) Plane section of real snow with ice shown in black, and the path of a hypothetical, point-like penetration into that snow structure in red.

During these campaigns, large snow blocks 30 cm × 30 cm × 100 cm were cut out in the field, packed into isolating Styrofoam boxes and transported at −30°C to the cold lab Davos, were they were measured simultaneously by SMP and CT in the cold lab at −25°C (after several weeks). For this study we used two of these block from Point Barnola and another two blocks from Kohnen Station. The Antarctic data set consists mainly of strongly metamorphosed faceted snow and depth hoar, with very low SSA and high density (Table 1).

All micro-CT measurements were performed in the cold lab in Davos. Two profiles of vertically overlapping cylindrical micro-CT samples were taken as shown in Figure 2c and then stitched together to create a continuous profile. Thereby, each cylinder has a height of 6.0 cm and a diameter of 3.6 cm and was completely measured by micro-CT. Vertical variations in the reconstructed volume are accounted for by analyzing the cylinder in a vertically moving window with $w^{(ct)} = 1.0$ cm and 50% overlap, where the overlapping areas were averaged.

For each of the four snow blocks, two SMP measurements were conducted and the derived parameters $L$ and $\tilde{F}$ (cf. section 2.2.1) were averaged vertically to 1 cm resolution with 50% overlap in order to match the resolution of the micro-CT derived parameters.

### 3.3. Arctic Snow
The Arctic snow data was gathered during the Nordic Snow and Radar Experiment (NoSREx) of the European Space Agency (ESA) hosted at the Finish Meteorological Institute in Sodankylä, Finland, during winter 2011/2012. The Arctic data set consists of three full-depth micro-CT sampled profiles with one SMP measurement per profile, Figure 2b. The maximum distance between SMP and micro-CT measurement was 50 cm. SMP measurements were conducted in situ in the field, while the micro-CT samples were cast simultaneously in the field and afterward analyzed in the cold lab following the replica technique of *Heggli et al.* [2009]. The remaining negative structure is imaged in the micro-CT in portions of $1 \times 1 \times 7$ cm$^3$. Vertical variations are accounted for by retrieving the micro-CT parameters in a moving window with $w^{(ct)} = 5.12$ mm and 50% overlap. Both SMP and micro-CT derived parameters profiles were then averaged to 1 cm window size with 50% overlap, to match the resolution of the micro-CT.

### 3.4. Matching SMP and Micro-CT Data
To generate corresponding pairs of micro-CT and SMP values it is necessary to match SMP and micro-CT derived profiles for the Arctic and Antarctic data sets. This was accomplished by aligning main stratigraphic features (crusts, ice lenses, and peaks in density and in correlation length). As layers in a natural snowpack are not perfectly parallel, a slight misalignment between SMP and micro-CT derived profiles cannot be excluded. However, we did not perform any stretching or compressing of layers. Both Antarctic and Arctic micro-CT profiles were averaged to 1 cm vertical resolution in order to smooth the stratigraphy to reduce the impact of layer misalignment. For the Alpine data, the SMP derived parameters were averaged vertically and over all four horizontal positions of the snow sample and then compared to the micro-CT measurement in the center.
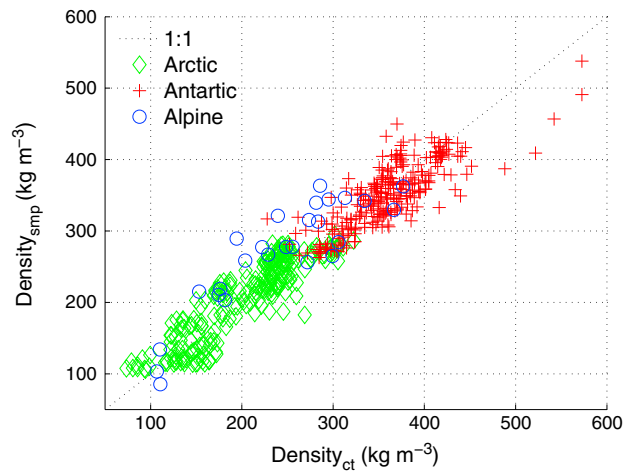
**Figure 4.** Scatterplot of SMP derived density $\rho^{(smp)}$ versus micro-CT derived density $\rho^{(ct)}$ for the three different data sets (colored symbols), with $R^2 = 0.90$ and RMSE = 30.1 kg m$^{-3}$. Derived from the median penetration force $\widetilde{F}$ and the SMP element size $L$ (see equation (9)) is $\rho^{(smp)}$. The dashed line serves as guide for the eye.

## 4. Results

### 4.1. Statistical Models

#### 4.1.1. SMP Derived Density $\rho^{(smp)}$

The first statistical model for the snow density derived from SMP measurements was published by *Pielmeier* [2003]. This model relates the logarithm of the median penetration force $\ln(\widetilde{F})$ to the snow density. *Marshall and Johnson* [2009] noticed that this model does not apply to all snow types and speculated that the integration of microstructural parameters will improve the density estimation. We modified this model and included the structural element size $L$ as an additional microstructural parameter into the regression. We used a bilinear regression model to relate the SMP variables $\ln(\widetilde{F})$ and $L$ to the micro-CT density $\rho^{(ct)}$, yielding an estimate for the density from the SMP

$$\rho^{(smp)} = a_1 + a_2 \ln(\widetilde{F}) + a_3 \ln(\widetilde{F})L + a_4 L \qquad (9)$$

with $a_1 = 420.47 \pm 8.31$ kg m$^{-3}$, $a_2 = 102.47 \pm 4.24$ N$^{-1}$, $a_3 = -121.15 \pm 10.65$ N$^{-1}$ mm$^{-1}$, and $a_4 = -169.96 \pm 18.70$ mm$^{-1}$, with respect to a 95% confidence interval. Figure 4 shows the correlation between $\rho^{(smp)}$ derived via equation (9) and micro-CT derived $\rho^{(ct)}$, with a coefficient of determination $R^2$ of 0.90 at a significance level of $p < 10^{-3}$. The root-mean-squared error (RMSE) is 30.1 kg m$^{-3}$ which corresponds to a relative error of 10.6% (RMSE divided by the mean of $\rho^{(ct)}$). The $R^2$ is 0.78, 0.80, and 0.64 for the density and has a relative error of 14.8%, 12.2%, and 8.5% for the Alpine, Arctic, and Antarctic data, respectively (cf. Table 2).

#### 4.1.2. SMP Derived Exponential Correlation Length $l_{ex}^{(smp)}$

To put forward a SMP estimate for the correlation length $l_{ex}$ we used the SMP element size $L$ as the main variable. As outlined in section 2.2.3 we relate the element size $L$ to the length scales derived from micro-CT, given the interpretation of $L$ as mean distance between two elements. Already a direct comparison between the correlation length $l_{ex}^{(ct)}$ and the element size $L$ shows a good correlation (Figure 5); however, the high-density Antarctic samples (red crosses) show too large $l_{ex}^{(ct)}$ values for the corresponding $L$ values. As the Antarctic samples are much denser, we account for such a "density effect" in the statistical model. To this end, a linear regression was carried out to relate the micro-CT correlation lengths $l_{ex}^{(ct)}$ to the SMP variables $L$ and $\ln(\widetilde{F})$ via

$$l_{ex}^{(smp)} = b_1 + b_2 L + b_3 \ln(\widetilde{F}) \qquad (10)$$

with $b_1 = 0.0715 \pm 0.0058$ mm, $b_2 = 0.299 \pm 0.011$ mm$^{-1}$, and $b_3 = 0.0149 \pm 0.0018$ N$^{-1}$.

**Table 2.** Statistical Measures for the Different Data Set and Parameters Used in This Study[a]

| Data Set | Density | | | Correlation Length | | SSA | |
| --- | --- | --- | --- | --- | --- | --- | --- |
| | $R^2$ | RMSE (kg m$^{-3}$) | $R^2$ | RMSE (mm) | $R^2$ | RMSE (mm$^{-1}$) | |
| Alpine | 0.78 | 35.9 (14.8%) | 0.91 | 0.026 (17.2%) | 0.85 | 4.03 (21.7%) | |
| Arctic | 0.80 | 24.9 (12.2%) | 0.87 | 0.029 (19.6%) | 0.83 | 4.04 (19.9%) | |
| Antarctic | 0.64 | 30.6 (8.5%) | 0.85 | 0.026 (12.3%) | 0.44 | 1.76 (19.9%) | |
| Overall | 0.90 | 30.1 (10.6%) | 0.86 | 0.029 (16.4%) | 0.86 | 3.39 (23.1%) | |

[a]RMSE is additionally given as percentage of the mean of the micro-CT derived values, which denotes the relative error. The significance levels for all data sets and parameters are $p < 10^{-3}$.
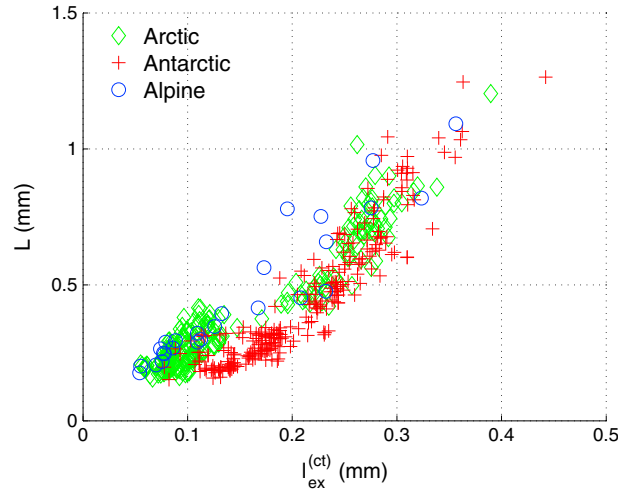
**Figure 5.** Scatterplot of SMP derived structural element size $L$ versus micro-CT derived exponential correlation length $l_{ex}^{(ct)}$ for the three different data sets (colored symbols). With exception for the higher-density Antarctic samples (red crosses), where the $L$ values tend to be too low in general, $l_{ex}^{(ct)}$ and $L$ are in good agreement ($R^2 = 0.79$).

Figure 6 shows the correlation between $l_{ex}^{(smp)}$ derived via equation (10) and micro-CT derived $l_{ex}^{(ct)}$, with $R^2 = 0.86$ at a significance level of $p < 10^{-3}$. The RMSE is 0.029 mm, which corresponds to a relative error of 16.4%. The deviation of the high-density samples in Figure 5 is corrected. The exponential correlation length is derived with $R^2$ of 0.91, 0.87, and 0.85 and with a relative error of 17.2%, 19.6%, and 12.3% for the Alpine, Arctic, and Antarctic data, respectively (Table 2).

### 4.1.3. SMP Derived Specific Surface Area SSA$^{(smp)}$

Finally we calibrated the statistical model of equation (10) again, but this time to predict the slope of the correlation function $l_c^{(ct)}$ at the origin instead of the exponential correlation length $l_{ex}^{(ct)}$. This leads to a regression model

$$l_c^{(smp)} = c_1 + c_2 L + c_3 \ln(\widetilde{F}) \tag{11}$$

with $c_1 = 0.131 \pm 0.0081$ mm, $c_2 = 0.355 \pm 0.015$ mm$^{-1}$, and $c_3 = 0.0291 \pm 0.0024$ N$^{-1}$. $R^2$ is 0.84 at a significance level of $p < 10^{-3}$. The RMSE is 0.041 mm which corresponds to a relative error of 16.7%.

The statistical relation enables to derive the SSA directly from SMP measurements, by substituting $l_c^{(smp)}$ from equation (11) and $\phi^{(smp)} = \rho^{(smp)} / \rho_{ice}$ with $\rho^{(smp)}$ from equation (9) to equation (4)

$$SSA^{(smp)} = \frac{4(1 - \phi_i^{(smp)})}{l_c^{(smp)}} \tag{12}$$

Figure 7 shows the correlation between SSA$^{(smp)}$ and SSA$^{(ct)}$ with $R^2 = 0.86$ at a significance level of $p < 10^{-3}$. The RMSE is 3.39 mm$^{-1}$ which corresponds to a relative error of 23.1% on average. The SSA is derived with $R^2$ of 0.85, 0.83, and 0.44 and with a relative error of 21.7%, 19.9%, and 19.9% for the Alpine, Arctic, and Antarctic data, respectively (Table 2).

Note that we have computed the SSA from the slope of the correlation function (section 2.1.1) since this method was available for all data. To provide some confidence that this estimate is basically equivalent to the surface triangulation of the reconstructed 3-D structure [*Hildebrand et al.*, 1999], we show the comparison for both methods in Figure 8 for the Alpine data, which is the only data set where both methods are available. Both methods to derive the SSA lead to very similar results, with $R^2 = 0.996$ and RMSE = 0.67 mm$^{-1}$.
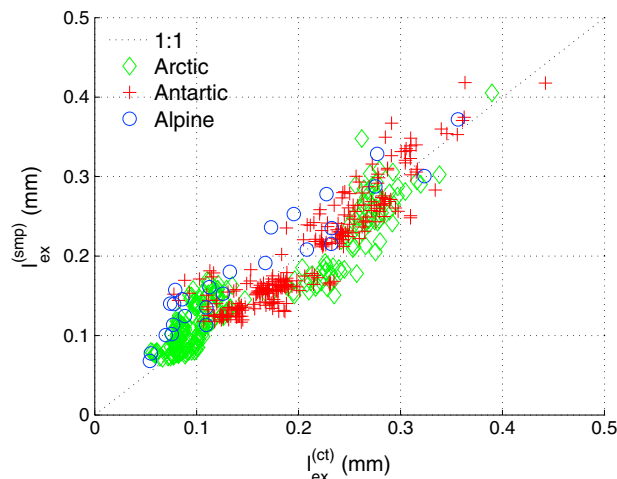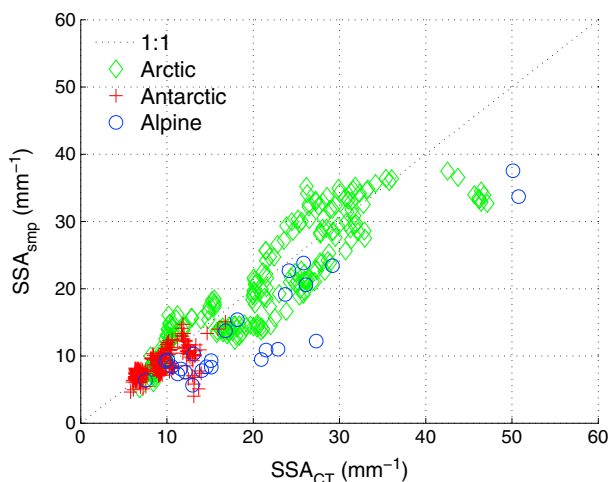


**Figure 6.** Scatterplot of SMP derived exponential correlation length $l_{ex}^{(smp)}$ versus micro-CT derived exponential correlation length $l_{ex}^{(ct)}$ for the three different data sets (colored symbols), with $R^2 = 0.86$ and RMSE = 0.029 mm. Derived from the SMP element size $L$ and density $\rho^{(smp)}$ (see equation (10)) is $l_{ex}^{(smp)}$. The dashed line serves as guide for the eye.

**Figure 7.** Scatterplot of SMP derived SSA$^{(smp)}$ versus micro-CT derived SSA$^{(ct)}$ for the three different data sets (colored symbols), with $R^2 = 0.86$ and RMSE = 3.34 mm$^{-1}$. SSA$^{(smp)}$ is derived from the SMP element size $L$ and density $\rho^{(smp)}$ (see equations (11) and (12)). The dashed line serves as guide for the eye.

### 4.2. Model Comparison for Two Vertical Profiles

Here we compare the statistical model to the micro-CT measurements on independent data for two vertical profiles, one from the Arctic and one from the Antarctic.

Figure 9 shows the micro-CT and SMP derived density, exponential correlation length, and SSA for one of the Antarctic snow blocks from Point Barnola. The corresponding $R^2$ is 0.55, 0.71, and 0.15, with $p < 10^{-3}$, $p < 10^{-3}$, and $p < 10^{-2}$, respectively, for all three parameters. The complex density and correlation length patterns are reproduced in detail by the SMP, whereas the SSA profile was not recovered as precisely as the other parameters. Note the very small SSA for the Antarctic data in general.

Slight horizontal variability was visible for this small snow block (approximately 20 cm in width). The single SMP signals (blue and red dashed lines in Figure 9) revealed deviations of stratigraphic features. For instance, the peak in correlation length at 75 mm snow depth had a 15 mm shift in the two SMP signals. For the region between 150 mm and 200 mm snowdepth the density and correlation length of both methods coincided very precisely.

Figure 10 shows the micro-CT and SMP derived density, exponential correlation length, and SSA for an Arctic profile measured during NoSREx III in Sodankylä, Finland. The corresponding $R^2$ is 0.82 for the density, 0.92 for the correlation length, and 0.86 for the SSA, respectively, with $p < 10^{-3}$ for all three parameters. The transition from new to old snow at 300 mm snow depth was captured by the SMP in terms of density and correlation length. For SSA$^{(smp)}$ this transition was less distinct. For the topmost 50 mm the SMP slightly overestimated the density and the correlation length but underestimated the SSA.

### 4.3. Model Validation
Besides the profile comparison shown in the previous section we have also compared the SMP and micro-CT
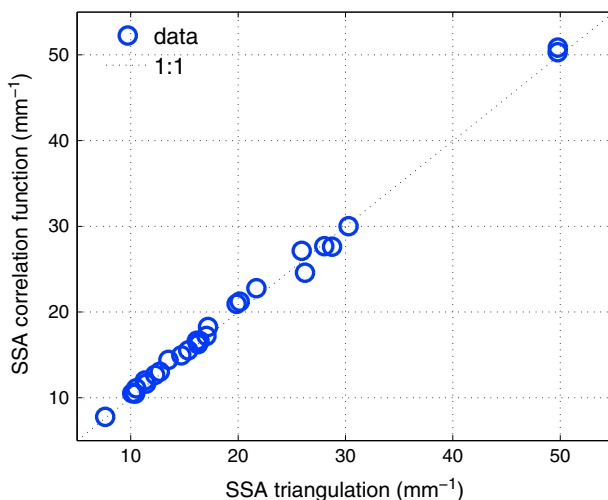


**Figure 8.** SSA measured by micro-CT using surface triangulation versus SSA calculated from the slope at the origin of the correlation function for the Alpine data set.

derived parameters on the basis of two vertical profiles which were obtained by different methods. For one profile the SSA was measured by near-infrared photography (NIP) following *Matzl and Schneebeli* [2006] and the density was measured traditionally with a 100 cm$^3$ density cutter (Figure 10). The NIP derived SSA is in good agreement with the SMP derived SSA$^{(smp)}$ ($R^2 = 0.93$, $p < 10^{-3}$). This points toward an effect of spatial variability with regard to the underestimation of SSA$^{(smp)}$ mentioned above: the NIP measurements were performed in between the SMP and micro-CT measurement, so that the topmost micro-CT sample could already be taken from slightly less dense and higher SSA snow. Further, $R^2$ is 0.82 ($p < 10^{-3}$) between NIP and micro-CT
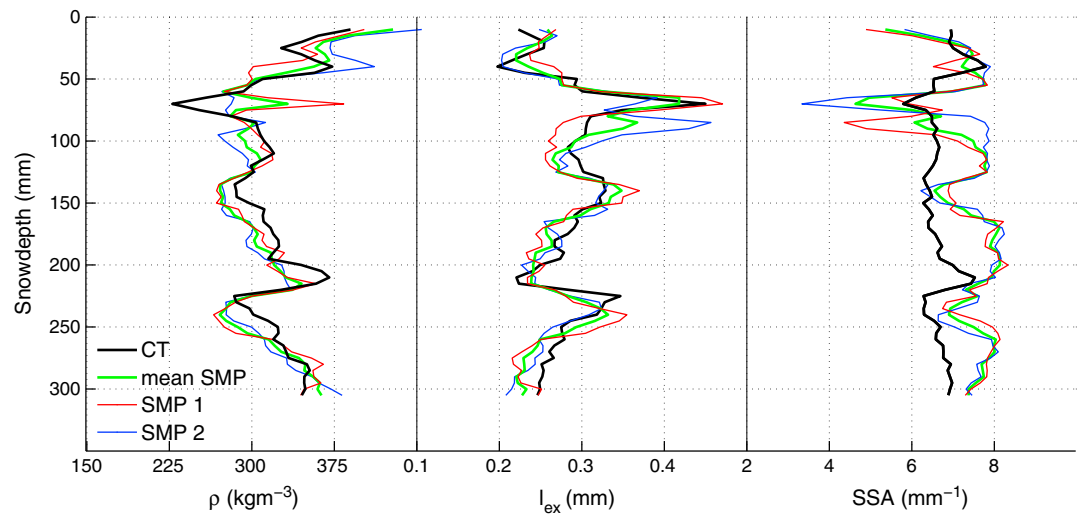
**Figure 9.** Density $\rho$, exponential correlation length $l_{ex}$, and SSA profile of an Antarctic snow block from Point Barnola, measured in the cold lab of SLF, by micro-CT (black) and SMP (blue and red). The green line represents the average of the two SMP measurements.

derived SSA which is lower than between SMP and NIP. The low SSA values from NIP at the very bottom are caused by shading due to the concave shape of the profile, where the loose depth hoar grains are dropping out during the sawing process.

The hand density measured with the density cutter is also in good agreement with $\rho^{(smp)}$ ($R^2 = 0.87$, $p < 10^{-3}$) and $\rho^{(ct)}$ ($R^2 = 0.82$, $p < 10^{-3}$). The low values for snow depth deeper than 600 mm are an artifact of sampling depth hoar with the density cutter: the fragile snow structure got destroyed while inserting the density cutter allowing loose snow grains to drop out of the cutter, which reduced the total weight of the filled cutter and, in turn, the measured density.

In addition, we compare the SMP derived and manually measured densities for an Alpine snow profile performed in the Steintälli above Davos, Switzerland, on 13 February 2014 (Figure 11). Two SMP signals close to the manual profile were averaged and compared to the densities of the snow layers measured with a density cutter. Both measurement techniques are in good agreement. The SMP densities, derived with a
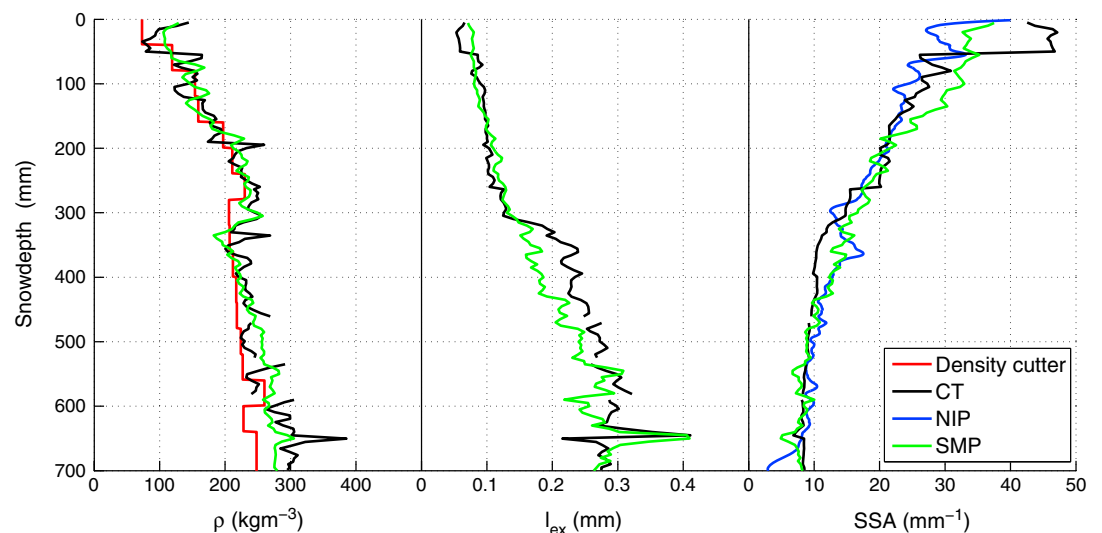


**Figure 10.** Density $\rho$, exponential correlation length $l_{ex}$, and SSA profile measured in the field during NoSREx III in Sodankylä, Finland, by micro-CT (black) and SMP (green). In addition, the density measured by hand with a 100 cm³ density cutter (red) and the SSA measured by near-infrared photography (NIP) (blue) are shown.
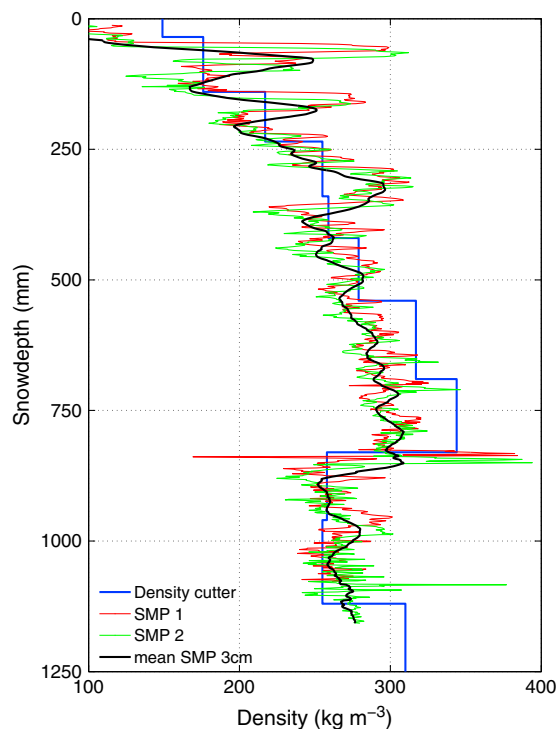
**Figure 11.** Density measured by a 100 cm³ density cutter (black) and SMP (green and grey) in the Steintälli above Davos, Switzerland. The black line is the average of the two neighboring SMP measurements.

vertical resolution of 1.25 mm and also averaged to 3 cm, reveal even smallest density variations, which the density cutter did not resolve.

### 4.4. Model Application: Retrieval of Two-Dimensional Stratigraphy

Next we applied the model to derive a quantitative characterization of the two-dimensional stratigraphy of a 1.1 m deep and 46 m long snow and firn transect measured in December 2012 at Kohnen Station, Antarctica. Along the transect, 92 SMP measurements were taken with 0.5 m intervals. Figure 12 shows the two-dimensional image of the SMP derived density obtained by assembling the parameter estimates from all 92 profiles. The stratigraphy revealed typical features of the snow and firn in the region of Kohnen Station. Six to seven main layers could be identified, each between 5 cm and 30 cm thick. The layers were horizontally undulated and dune-shaped, indicating a strong wind influence.

## 5. Discussion

### 5.1. Overall Performance of the Method

To assess the retrievals of density, correlation length, and SSA of snow solely from SMP measurements, we first discuss the errors obtained from the statistical model by taking micro-CT as reference values. The SMP derived density, correlation length, and SSA are correlated linearly to their micro-CT derived counterparts, with a relative error of 10.6%, 16.4%, and 23.1%, respectively.

Comparing the relative errors between data sets, the smallest relative error was found for the Antarctic data set, where the density is predicted within 8.5%, the correlation length within 12.3% and the
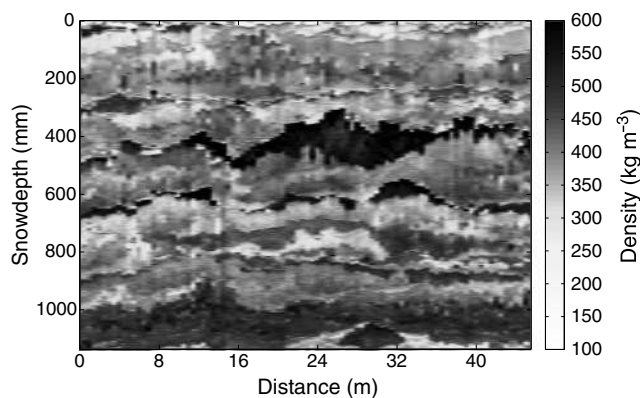


**Figure 12.** SMP derived density $\rho^{(smp)}$ for a 46 m long and 1.1 m deep snow and firn transect measured during December 2012 at Kohnen Station, Antarctica. The figure is a composite of 92 SMP measurements with 0.5 m interval. The deposition features are highly complex, with layers of variable thickness and noncontinuous layers like the "whale-back" structure between 300 mm and 600 mm snowdepth reaching from 16 m to 38 m in the vertical direction.

SSA within 19.9% on average. The lower errors for the Antarctic data set can be explained by the absence of low-density samples in this data set. For low-density snow higher errors are expected, due to a poor signal-to-noise ratio for the SMP when approaching densities of 50 kg m⁻³ [*Schneebeli et al.*, 1999]. In addition, the distance between SMP and micro-CT measurements was smallest for the Antarctic data set, which minimized the error by layer misalignment. This uncertainty due to spatial variability is inherent to the method and discussed later in detail.

Comparing the relative error between different quantities, the density showed the best performance with

the smallest relative error (10.6%), while the SSA has the largest error (23.1%) on average. The difference in performance can be partly attributed to the fact that SSA is a derived parameter (equation (12)) which involves two SMP regressions, namely $\rho^{(smp)}$ and $l_c^{smp}$, which are both subject to individual scatter.

The error in SSA$^{(smp)}$ is larger than SSA measured with other methods, which is typically in the range of 10 and 15%. For NIR photography [*Matzl and Schneebeli*, 2006] the estimated error is 15%, for IRIS and SWIRcam [*Montpetit et al.*, 2012] 10%, for DUFISSS [*Gallet et al.*, 2009] below 12%, and for POSSSUM [*Arnaud and Picard*, 2011] between 10 and 15%. For the density, our method performs equally well as other methods. *Conger and McClung* [2009] report a variation of densities measured with different types of density cutters of 11%, whereas the variation within the individual cutter types reached up to 6.2%. An error comparison for the correlation length is difficult, since it can be derived only from three-dimensional micro-CT reconstruction [e.g., *Löwe et al.*, 2011] or surface sections [e.g., *Wiesmann et al.*, 1998]. A comparison of both methods and error estimates is not available.

The discussion above shows that our method performs comparably well or slightly worse than other existing methods for the SSA and density. The clear benefit of the method becomes obvious only in combination with a discussion of measurement times and vertical resolution. Besides IR profiling techniques such as POSSSUM [*Arnaud and Picard*, 2011] or GPR systems, all other existing snow measurement methods require to excavate a snow pit or trench, which constitutes the major time constraint for the method. For IR profiling a hole has to be drilled in advance, which takes around 20 min for 2 m depth [*Arnaud and Picard*, 2011]. Though GPR systems are able to provide continuous stratigraphic information over a large extent without time consuming profile preparation [*Marshall et al.*, 2007], the method still lacks a convenient retrieval of the density [*Schmid et al.*, 2014], let alone the SSA or correlation length. IR techniques are able to provide two-dimensional SSA profiles on the meter scale [*Tape et al.*, 2010] but lack the retrieval of density. For a further discussion of snow measurement methods we refer to *Proksch and Schneebeli* [2012].

Given the advantages and disadvantages of other methods, we consider our SMP-based method for a combined retrieval of density, SSA, and correlation length profiles in less than a minute a powerful alternative. Before turning to the application of the method, we will discuss the origin of the errors and potential improvements of the method.

### 5.2. Error Analysis
### 5.2.1. Limitations of the Micropenetration Model
One error source is the theoretical model used to interpret the penetration force in snow and its relation to the microstructural length scale *L*. Understanding details of the indentation process is challenging and less obvious than the relation of IR reflectivity to SSA. One basic assumption of the model [*Löwe and van Herwijnen*, 2012; *Johnson and Schneebeli*, 1999] is the superposition of the SMP force signal by spatially uncorrelated element failures. This is a very simplistic though practical assumption. The higher the density, the higher the probability that a failed element interacts with other elements, leading to a violation of the basic assumption of the model. This is the reason why we empirically included the median of the penetration force as a factor for density in our model for the correlation length. This improved the results significantly (Figure 6) in comparison to the minimal approach of comparing the SMP length scale *L* directly with the correlation length $l_{ex}$ (Figure 5).

Taking into consideration the aspect discussed above, we have also included the length scale *L* in our model for the density (equation (9)) which can be regarded as an extension of the original idea from *Marshall* [2005], which was solely based on the median of the penetration force. Using only the median of the force, the regression model was less accurate, in particular for highly metamorphosed structures. Without including *L*, the density would have been 40% too low for the depth hoar layers in Sodankylä when compared to the micro-CT or hand-measured density. This can be attributed to the low penetration force in very fragile snow types such as depth hoar where ice structures are broken easily in contact with the SMP tip. In this case the median penetration force in depth hoar is relatively small compared to other snow types of the same density. Since the element size *L* is rather large in depth hoar, the inclusion of *L* can discriminate these cases and correct the density estimates. We expect that improvements in the theory of the penetration process will reduce the errors of the present statistical model.

Another point not addressed in the current model is the anisotropy of the snow structure. It is now well known that the snow structure is anisotropic [*Riche and Schneebeli*, 2013]. The micropenetration model used here has no provision for anisotropy, and we are therefore unable to quantify effects of anisotropy on the

measurements and the data. A quantification of this effect will again require a substantial improvement in the theory of the penetration process, or numerical simulations and measurements in snow of similar correlation length, but a varying degree of anisotropy.

### 5.2.2. Limitations Arising From Data Acquisition

Besides the limitations of the micropenetration model, uncertainties in our method also arise from the data acquisition, in particular due to the inclusion of field data in the regression. The inclusion of field data of Alpine, Arctic, and Antarctic snow was necessary to show that the method is representative for a broad range of densities and SSA. By the inclusion of field data, spatial variability in horizontal and vertical directions acted as an additional error source. In the field, SMP measurements and micro-CT samples cannot be taken exactly at the same position, and thus, the spatial variability introduced uncertainty in our data. This situation is somewhat different from previous comparisons of different methods. For the lab-based SSA study [*Matzl and Schneebeli*, 2010], the authors found a very high correlation between the SSA derived from micro-CT and stereology ($R^2 = 0.99$, $p \ll 0.01$) and gas adsorption ($R^2 = 0.96$, $p \ll 0.01$), respectively. In these cases, the different methods were applied to exactly the same sample. This eliminates the error source of spatial variability and leads to higher correlation coefficients.

The Arctic data set is most affected by spatial variability, with the largest distance between micro-CT and SMP measurements, and just one SMP measurement per micro-CT sampled profile (Table 1). In contrast, the Antarctic snow samples were brought to the lab which allowed to reduce the distance between micro-CT and SMP measurements and a better control of the alignment of the layers. Two SMP measurements around the location of the respective micro-CT samples were performed and averaged, further reducing errors from horizontal variability. However, Figure 9 reveals small-scale variability even in the carefully prepared Antarctic snow blocks where the two SMP signals showed slight differences in the location of pronounced stratigraphic features. Horizontal variability was also present for the Alpine data set despite the SMP averaging over four measurements (section 3.1). The effect of spatial variability is inherent to all snow measurements methods and will affect any intercomparison of destructive methods.

Another technical limitation of the statistical model presented here is the incompatibility with the newest hardware version of the SMP. We detected that a small change in the A/D conversion of the force signal leads to different values in the structural element size $L$. This will be resolved either by providing a new calibration or by adjusting the A/D conversion for the SMP version 4.

### 5.3. Spatial Variability and Retrieval of Two-Dimensional Stratigraphy

Overall, the errors discussed in the previous section are still smaller than the variations of the parameters we found in the analysis of the two-dimensional stratigraphy shown in Figures 12 to 14. It is thus reasonable to interpret these as true features of the stratigraphy and discuss their implication.

The importance of two-dimensional stratigraphy was already demonstrated by *Benson* [1971]. Our two-dimensional plots clearly reveal the horizontal heterogeneity of the snow and firn at Kohnen Station, Antarctica. The layers show a horizontally undulated pattern. These patterns are likely due to snow redistribution under the strong influence of wind, as mentioned in several studies [*Gow*, 1965; *Alley*, 1988; *Birnbaum et al.*, 2010]. The layers indicate major depositional and metamorphic events of the last years, which are mostly separated by very thin high density, crust-like layers less than 2 cm thick. Also, thicker layers of high density are present, which have been referred to as whale-back layers in the literature [*Gow*, 1965]. The importance of these layers for firn processes has been highlighted, e.g., by *Birnbaum et al.* [2010] and *Freitag et al.* [2002]. The layers are able to limit air permeability and the mixing of air by advection, with consequences for the interpretation of ice-core records. The density patterns coincide also with the correlation length and SSA patterns as shown in Figures 13 and 14. The high-density whale-back and crust-like structures correspond also to a higher correlation length and a lower SSA.

The advantages of our method become obvious in the presented Kohnen example: No trench had to be dug for the two-dimensional stratigraphic information shown in Figures 12 to 14. The data were derived from 92 SMP measurements which were conducted in half a day, which is very fast compared to digging a 46 m long and 1.1 m trench in Antarctic snow. Fast measurement times are an asset in harsh polar environments, and they further enable repeated measurements in order to reduce uncertainties by spatial variability.
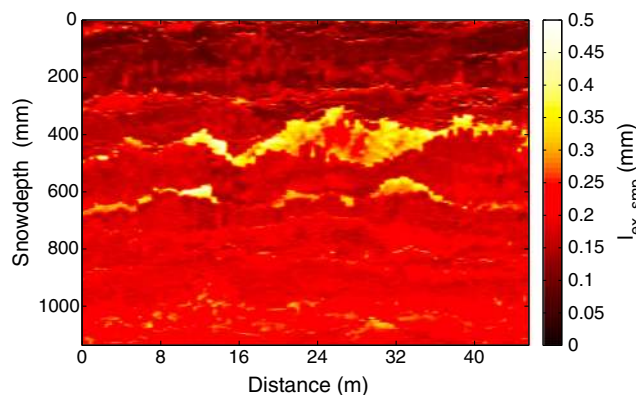
**Figure 13.** Same as Figure 12 but for SMP derived correlation length $l_{ex}^{(smp)}$.

But also other applications might benefit from a high-resolution retrieval of 2-D stratigraphy. *Köchle and Schneebeli* [2014] mentioned the limited resolution of a traditional snow profile as a major drawback for the characterization of weak layers. *Monti et al.* [2012] showed that the validation of snow cover models is complicated due to the higher number of simulated than observed layers. And finally for the application to remote sensing, *Rutter et al.* [2014] has recently raised the issue of 2-D stratigraphy explicitly. Implications for microwave remote sensing are discussed below.

### 5.4. Relevance for Microwave Remote Sensing

For microwave remote sensing, brightness temperatures spectra observed in Antarctica cannot be explained with a homogeneous snowpack but depend on the vertical resolution of the input profile [*Brucker et al.*, 2011]. *Durand et al.* [2011] has shown that the RMSE in retrieved snow height approaches 50% when stratigraphy is neglected. *Havens et al.* [2013] pointed out that remote sensing of snow could benefit from the ability of the SMP to quickly quantify stratigraphic information. The authors provided a framework to classify the grain type, with respect to *Marshall et al.* [2007], who showed that ground-based radar reflections are associated with layer boundaries seen in SMP measurements. With the present approach we were able to provide even quantitative information for the correlation length $l_{ex}$ and the density from the SMP. These two parameters can be directly used as complete stratigraphic input for microwave models such as the Microwave Emission Model of Layered Snowpacks (MEMLS) [*Wiesmann and Mätzler*, 1999]. This is a key step for the inclusion of extensive ground truth measurements to improve microwave remote sensing modeling for global snow water equivalent (SWE) retrieval.

But also for models which do not require $l_{ex}$ explicitly as input parameter, the method is a progress. For single-layer models, frequently applied in operational use or for climate research purposes [*Luojus et al.*, 2010], meaningful mean values of snowpack parameters must be derived. High-resolution measurements are needed to develop the weighting formulas to condense the stratigraphic information into one single number and to better interpret the physical meaning of grain size parameterization in such models.

As a final note, we have provided a first answer to an old question posed by *Vallese and Kong* [1981] "Is there a way of obtaining [...] the specific correlation functions by a proper analysis of the ground truth data [...]?" The exponential correlation length is only a simpli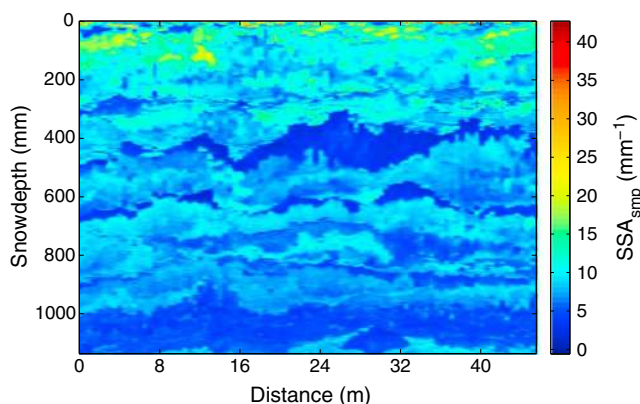fied characterization of correlation functions in snow [*Löwe et al.*, 2011], but we believe that other relevant length scales could be retrieved by a generalization of the presented method.

### 6. Conclusions

We developed a first statistical approach to estimate three major snow structural parameters, the density, the exponential correlation length, and the SSA solely from SMP measurements. Our data set covers a broad range of densities and SSA and includes Arctic, Antarctic, and Alpine snow. We found the SMP derived parameters to be linearly correlated



**Figure 14.** Same as Figure 12 but for SMP derived specific surface area SSA$^{(smp)}$.

to their micro-CT derived counterparts within 10.6%, 16.4%, and 23.1% for density, correlation length and SSA, respectively. For the high-density Antarctic snow data set alone, those parameters are derived more accurately, within 8.5%, 12.3%, and 19.9%, respectively. If time and cost are available, researchers are able to assimilate their own data to calibrate the instrument based on their particular needs, e.g., by including NIR SSA or manual density measurements.

The fact that a strong relation between SMP and micro-CT derived parameters exists for such a broad range of densities and SSA supports the approach to derive not only micromechanical but also microstructural parameters from SMP measurements and to set up the SMP as an alternative, high-resolution, and objective tool to derive snow structural parameters.

Deriving quantitative information with high resolution in an observer independent way, the SMP enables an unambiguous investigation of the snow microstructure and its variability. Through repeated measurements, the two-dimensional stratigraphy of snow and firn can be derived in a quantitative way. We therefore believe that the method could be beneficial for a wide range of applications such as the determination of the snow and firn stratigraphy as well as the calibration and validation of snow cover or microwave models. All these applications rely on quantitative snow measurements. A fast and high-resolution method which allows the combined measurement of density and SSA or correlation length is not yet available to our knowledge. Being portable and taking full-meter profiles in less than 1 min, this method is particularly feasible for the operation in harsh polar environments or during extensive ground truth campaigns.

## References

Alley, R. B. (1988), Concerning the deposition and diagnosis of strata in polar firn, *J. Glaciol.*, *34*(118), 283–290.

Arcone, S. A., R. Jacobel, and G. Hamilton (2012), Unconformable stratigraphy in East Antarctica: Part I. Large firn cosets, recrystallized growth, and model evidence for intensified accumulation, *J. Glaciol.*, *58*(208), 240–252, doi:10.3189/2012JoJ11J044.

Arnaud, L., and G. Picard (2011), Measurement of vertical profiles of snow specific surface area with a 1 cm resolution using infrared reflectance: Instrument description and validation, *J. Glaciol.*, *57*(201), 17–29.

Arons, E. M., and S. C. Colbeck (1995), Geometry of heat and mass transfer in dry snow: A review of theory and experiment, *Rev. Geophys.*, *33*(4), 463–493, doi:10.1029/95RG02073.

Bellaire, S., C. Pielmeier, M. Schneebeli, and J. Schweizer (2009), Instruments and methods: Stability algorithm for snow micro-penetrometer measurements, *J. Glaciol.*, *55*(193), 805–813, doi:10.3189/002214309790152582.

Benson, C. (1971), Stratigraphic studies in snow at Byrd Station, Antarctica, compared with similar studies in Greenland, in *Antarctic Snow and Ice Studies II*, vol. 16, pp. 333–353, AGU, Washington, D. C.

Berryman, J. G. (1987), Relationship between specific surface area and spatial correlation functions for anisotropic porous media, *J. Math. Phys.*, *28*(1), 244–245, doi:10.1063/1.527804.

Birnbaum, G., et al. (2010), Strong-wind events and their influence on the formation of snow dunes: Observations from Kohnen station, Dronning Maud Land, Antarctica, *J. Glaciol.*, *56*(199), 891–902, doi:10.3189/002214310794457272.

Brucker, L., G. Picard, L. Arnaud, J.-M. Barnola, M. Schneebeli, E. Lefebvre, and M. Fily (2011), Modeling time series of microwave brightness temperature at Dome C, Antarctica, using vertically resolved snow temperature and microstructure measurements, *J. Glaciol.*, *57*(201), 171–182, doi:10.3189/002214311795306736.

Calonne, N., C. Geindreau, F. Flin, S. Morin, B. Lesaffre, S. Rolland du Roscoat, and P. Charrier (2012), 3-D image-based numerical computations of snow permeability: Links to specific surface area, density, and microstructural anisotropy, *The Cryosphere*, *6*(5), 939–951, doi:10.5194/tc-6-939-2012.

Conger, S. M., and D. M. McClung (2009), Instruments and methods: Comparison of density cutters for snow profile observations, *J. Glaciol.*, *55*(189), 163–169, doi:10.3189/002214309788609038.

Debye, P., J. H. R. Anderson, and H. Brumberger (1957), Scattering by an inhomogeneous solid. II. The correlation function and its application, *J. Appl. Phys.*, *28*(6), 679–683, doi:10.1063/1.1722830.

Denoth, A., A. Foglar, P. Weiland, C. Mätzler, and H. Aebischer (1984), A comparative study of instruments for measuring the liquid water content of snow, *J. Appl. Phys.*, *56*(7), 2154–2160, doi:10.1063/1.334215.

Durand, M., E. Kim, and S. A. Margulis (2008), Quantifying uncertainty in modeling snow microwave radiance for a mountain snowpack at the point-scale, including stratigraphic effects, *IEEE Trans. Geosci. Remote Sens.*, *46*(6), 1753–1767, doi:10.1109/TGRS.2008.916221.

Durand, M., E. J. Kim, S. A. Margulis, and N. P. Molotch (2011), A first-order characterization of errors from neglecting stratigraphy in forward and inverse passive microwave modeling of snow, *IEEE Geosci. Remote Sens. Lett.*, *8*, 730–734, doi:10.1109/LGRS.2011.2105243.

Fierz, C., R. Armstrong, Y. Durand, P. Etchevers, E. Greene, D. McClung, K. Nishimura, P. Satyawali, and S. A. Sokratov (2009), The international classification for seasonal snow on the ground, *HP-VII Technical Documents in Hydrology N83, IACS Contribution N1, UNESCO-IHP, Paris*.

Freitag, J., U. Dobrindt, and J. Kipfstuhl (2002), A new method for predicting transport properties of polar firn with respect to gases on the pore-space scale, *Ann. Glaciol.*, *35*(1), 538–544, doi:10.3189/172756402781816582.

Gallet, J., F. Domine, C. Zender, and G. Picard (2009), Measurement of the specific surface area of snow using infrared reflectance in an integrating sphere at 1310 and 1550 nm, *The Cryosphere*, *3*, 167–182, doi:10.5194/tc-3-167-2009.

Gow, A. J. (1965), On the accumulation and seasonal stratification of snow at the South Pole, *J. Glaciol.*, *5*, 467–477.

Havens, S., H. P. Marshall, C. Pielmeier, and K. Elder (2013), Automatic grain type classification of snow micro penetrometer signals with random forests, *IEEE Trans. Geosci. Remote Sens.*, *51*(6), 3328–3335, doi:10.1109/TGRS.2012.2220549.

Heggli, M., E. Frei, and M. Schneebeli (2009), Instruments and methods. Snow replica method for three-dimensional X-ray microtomographic imaging, *J. Glaciol.*, *55*(192), 631–639, doi:10.3189/002214309789470932.

Hildebrand, T., A. Laib, R. Müller, J. Dequecker, and P. Rüegsegger (1999), Direct 3-D morphometric analysis of human cancellous bone: Microstructural data from spine, femur, iliac and calcaneus, *J. Bone Miner. Res.*, *14*(7), 1167–1174.

Johnson, J., and M. Schneebeli (1999), Characterizing the microstructural and micromechanical properties of snow, *Cold Reg. Sci. Technol.*, *30*(1–3), 91–100, doi:10.1016/S0165-232X(99)00013-0.

Köchle, B., and M. Schneebeli (2014), 3D microstructure and numerical calculation of elastic properties of Alpine snow with focus on weak layers, *J. Glaciol.*, *60*(222), 1–20.

Kronholm, K., M. Schneebeli, and J. Schweizer (2004), Spatial variability of micropenetration resistance in snow layers on a small slope, *Ann. Glaciol.*, *38*(1), 202–208, doi:10.3189/172756404781815257.

Löwe, H., and A. van Herwijnen (2012), A Poisson shot noise model for micro-penetration of snow, *Cold Reg. Sci. Technol.*, *70*, 62–70, doi:10.1016/j.coldregions.2011.09.001.

Löwe, H., J. K. Spiegel, and M. Schneebeli (2011), Interfacial and structural relaxations of snow under isothermal conditions, *J. Glaciol.*, *57*, 499–510, doi:10.3189/002214311796905569.

Löwe, H., F. Riche, and M. Schneebeli (2013), A general treatment of snow microstructure exemplified by an improved relation for thermal conductivity, *The Cryosphere*, *7*(5), 1473–1480, doi:10.5194/tc-7-1473-2013.

Luojus, K., et al. (2010), Investigating the feasibility of the Globsnow snow water equivalent data for climate research purposes, *2010 IEEE International Geoscience and Remote Sensing Symposium (IGARSS)*, Honolulu, doi:10.1109/IGARSS.2010.5741987.

Marshall, H. P. (2005), Snowpack spatial variability: Towards understanding its effect on remote sensing measurements and snow slope stability, PhD thesis, Department of Civil, Environmental, and Architectural Engineering, Univ. of Colo., Boulder.

Marshall, H. P., and J. B. Johnson (2009), Accurate inversion of high-resolution snow penetrometer signals for microstructural and micromechanical properties, *J. Geophys. Res.*, *114*, F04016, doi:10.1029/2009JF001269.

Marshall, H. P., M. Schneebeli, and G. Koh (2007), Snow stratigraphy measurements with high-frequency FMCW radar: Comparison with snow micro-penetrometer, *Cold Reg. Sci. Technol.*, *47*, 108–117, doi:10.1016/j.coldregions.2006.08.008.

Matzl, M., and M. Schneebeli (2006), Measuring specific surface area of snow by near-infrared photography, *J. Glaciol.*, *52*(179), 558–564, doi:10.3189/172756506781828412.

Matzl, M., and M. Schneebeli (2010), Stereological measurement of the specific surface area of seasonal snow types: Comparison to other methods, and implications for mm-scale vertical profiling, *Cold Reg. Sci. Technol.*, *64*(1), 1–8, doi:10.1016/j.coldregions.2010.06.006.

Mätzler, C. (1996), Microwave permittivity of dry snow, *IEEE Trans. Geosci. Remote Sens.*, *34*(2), 573–581, doi:10.1109/36.485133.

Mätzler, C. (1999), Extension of the microwave emission model of layered snowpacks to coarse-grained snow, *Remote Sens. Environ.*, *70*(3), 317–325, doi:10.1016/S0034-4257(99)00047-4.

Mätzler, C. (2002), Relation between grain-size and correlation length of snow, *J. Glaciol.*, *48*, 461–466.

Monti, F., A. Cagnati, M. Valt, and J. Schweizer (2012), A new method for visualizing snow stability profiles, *Cold Reg. Sci. Technol.*, *78*, 64–72, doi:10.1016/j.coldregions.2012.02.005.

Montpetit, B., A. Royer, A. Langlois, P. Cliche, A. Roy, N. Champollion, G. Picard, F. Domine, and R. Obbard (2012), New shortwave infrared albedo measurements for snow specific surface area retrieval, *J. Glaciol.*, *58*(211), 941–952, doi:10.3189/2012JoG11J248.

Painter, T., N. Molotch, M. Cassidy, M. Flanner, and K. Steffen (2007), Instruments and methods: Contact spectroscopy for determination of stratigraphy of snow optical grain size, *J. Glaciol.*, *53*(180), 121–127.

Picard, G., L. Brucker, A. Roy, F. Dupont, M. Fily, A. Royer, and C. Harlow (2013), Simulation of the microwave emission of multi-layered snowpacks using the Dense Media Radiative Transfer Theory: The DMRT-ML model, *Geosci. Model Dev.*, *6*(4), 1061–1078, doi:10.5194/gmd-6-1061-2013.

Pielmeier, C. (2003), Textural and mechanical variability of mountain snowpacks, PhD thesis, Univ. of Bern, Bern, Switzerland.

Pielmeier, C., and H.-P. Marshall (2009), Rutschblock-scale snowpack stability derived from multiple quality-controlled SnowMicroPen measurements, *Cold Reg. Sci. Technol.*, *59*(2–3), 178–184, doi:10.1016/j.coldregions.2009.06.005.

Proksch, M., and M. Schneebeli (2012), Development of snow retrieval algorithms for CoReH2O grain size estimator: Procedures for objective snow pack structure parameters, *Tech. Rep. 22830/09/NL/JC*, ESA-ESTEC, Noordwijk, Netherlands.

Pulliainen, J., J. Grandell, and M. Hallikainen (1999), HUT snow emission model and its applicability to snow water equivalent retrieval, *IEEE Trans. Geosci. Remote Sens.*, *37*(3), 1378–1390, doi:10.1109/36.763302.

Reuter, B., and J. Schweizer (2012), The effect of surface warming on slab stiffness and the fracture behavior of snow, *Cold Reg. Sci. Technol.*, *83–84*, 30–36, doi:10.1016/j.coldregions.2012.06.001.

Riche, F., and M. Schneebeli (2013), Thermal conductivity of snow measured by three independent methods and anisotropy considerations, *The Cryosphere*, *7*(1), 217–227, doi:10.5194/tc-7-217-2013.

Rutter, N., M. Sandells, C. Derksen, P. Toose, A. Royer, B. Montpetit, A. Langlois, J. Lemmetyinen, and J. Pulliainen (2014), Snow stratigraphic heterogeneity within ground-based passive microwave radiometer footprints: Implications for emission modeling, *J. Geophys. Res. Earth Surf.*, *119*, 550–565, doi:10.1002/2013JF003017.

Scambos, T. A., M. Frezzotti, T. Haran, J. Bohlander, J. T. M. Lenaerts, M. R. Van Den Broeke, K. Jezek, D. Long, S. Urbini, K. Farness, T. Neumann, M. Albert, and J.-G. Winther (2012), Extent of low-accumulation 'wind glaze' areas on the East Antarctic plateau: Implications for continental ice mas balance, *J. Glaciol.*, *58*(210), 633–647, doi:10.3189/2012JoG11J232.

Schleef, S., M. Jaggi, H. Löwe, and M. Schneebeli (2014), An improved machine to produce nature-identical snow in the laboratory, *J. Glaciol.*, *60*(219), 94–102, doi:10.3189/2014JoG13J118.

Schmid, L., A. Heilig, C. Mitterer, J. Schweizer, H. Maurer, R. Okorn, and O. Eisen (2014), Continuous snowpack monitoring using upward-looking ground-penetrating radar technology, *J. Glaciol.*, *60*(221), 509–525, doi:10.3189/2014JoG13J084.

Schneebeli, M. (2001), High-resolution penetrometry in the low-porosity material snow, in *Proc. Int. Workshop. Penetrometry in the Solar System*, edited by Kömle, N. I., et al., pp. 61–72, Verlag Österr. Akad. Wiss., Wien.

Schneebeli, M., and J. Johnson (1998), A constant-speed penetrometer for high-resolution snow stratigraphy, *Ann. Glaciol.*, *26*, 107–111.

Schneebeli, M., C. Pielmeier, and J. Johnson (1999), Measuring snow microstructure and hardness using a high resolution penetrometer, *Cold Reg. Sci. Technol.*, *30*(1–3), 101–114, doi:10.1016/S0165-232X(99)00030-0.

Schweizer, J., J. B. Jamieson, and M. Schneebeli (2003), Snow avalanche formation, *Rev. Geophys.*, *41*(4), 1016, doi:10.1029/2002RG000123.

Sturm, M., and C. Benson (2004), Scales of spatial heterogeneity for perennial and seasonal snow layers, *Ann. Glaciol.*, *38*(1), 253–260, doi:10.3189/172756404781815112.

Tape, K. D., N. Rutter, H. P. Marshall, R. Essery, and M. Sturm (2010), Instruments and methods recording microscale variations in snowpack layering using near-infrared photography, *J. Glaciol.*, *56*(195), 75–80, doi:10.3189/002214310791190938.

Torquato, S. (2002), *Random Heterogeneous Materials*, Springer, New York.

Vallese, F., and J. A. Kong (1981), Correlation function studies for snow and ice, *J. Appl. Phys.*, *52*(8), 4921–4925.

Wiesmann, A., and C. Mätzler (1999), Microwave emission model of layered snowpacks, *Remote Sens. Environ.*, *70*(3), 307–316, doi:10.1016/S0034-4257(99)00046-2.

Wiesmann, A., C. Mätzler, and T. Weise (1998), Radiometric and structural measurements of snow samples, *Radio Sci.*, *33*(2), 273–289.